land

MDPI

Article

Characterization of Biochar from Beach-Cast Seaweed and Its Use for Amelioration of Acid Soils

Eliana Cárdenas-Aguiar [1,2,*], Gabriel Gascó [1], Marcos Lado [2], Ana Méndez [3], Jorge Paz-Ferreiro [4] and Antonio Paz-González [2]

[1] Department of Agricultural Production, Universidad Politécnica de Madrid, Ciudad Universitaria, 28040 Madrid, Spain; gabriel.gasco@upm.es
[2] Centro Interdisciplinar de Química e Bioloxía CICA, As Carballeiras, s/n Campus de Elviña, University of Corunna, 15008 Corunna, Spain; marcos.lado@udc.es (M.L.); antonio.paz.gonzalez@udc.es (A.P.-G.)
[3] Department of Geological and Mining Engineering, Universidad Politécnica de Madrid, 28040 Madrid, Spain; anamaria.mendez@upm.es (A.M.)
[4] School of Engineering, RMIT University, Melbourne 3000, Australia; jorge.paz-ferreiro@rmit.edu.au
* Correspondence: eliana.cardenas@col.udc.es

Abstract: Limited knowledge is available regarding biochar (BC) obtained from beach-cast seaweed, which needs to be characterized to better prospect its potential applications. Beach-cast seaweed BCs were produced at two temperatures (300 and 600 °C) and two residence times (1 and 3 h). First, an extensive characterization of feedstock and their derived BCs was performed. Then, an incubation experiment was conducted to investigate the potential of these BCs as ameliorants in two acidic soils, classified as Umbrisols. Proximate and elemental analyses suggested the presence of more stable C structures in BCs at 600 °C with a high C, fixed carbon (FC) and low H, O and volatile matter (VM); additionally, thermogravimetric graphics showed less weight loss. Some features from the raw material were present in biochars obtained at 300 °C but absent at 600 °C. Dissolved organic carbon was much lower in BCs pyrolyzed at 600 °C than at 300 °C, suggesting the higher aromaticity of the former, allowing more resistance to water extraction. The breakdown of proteinaceous soluble materials after pyrolysis was revealed by fluorescence. Residence time caused minor effects in biochar properties compared to temperature. The soil pH and macronutrient availability of the two studied soils increased after beach-cast seaweed biochar addition.

Keywords: beach-cast seaweed; biochars; valorization; pyrolysis; soil amelioration

Citation: Cárdenas-Aguiar, E.; Gascó, G.; Lado, M.; Méndez, A.; Paz-Ferreiro, J.; Paz-González, A. Characterization of Biochar from Beach-Cast Seaweed and Its Use for Amelioration of Acid Soils. *Land* **2024**, *13*, 881. https://doi.org/10.3390/land13060881

Academic Editor: Xun Wang

Received: 10 May 2024
Revised: 5 June 2024
Accepted: 14 June 2024
Published: 18 June 2024

1. Introduction

Algae can be converted to chemicals, biofuels and materials; the commercial applications of algae are important in several fields, including energy, agriculture, and various industries, as, for example, pharmaceutical, food, textile, cosmetic, glass or paper [1]. In particular, algae have been identified recently as a valuable raw material to produce renewable fuels [2]. The world production of macroalgae (seaweed), on a dry matter basis, has been estimated at about 12 million t/year, while the microalgae contribution is much lower, around 9200 t/year [1].

Beach-cast seaweed accumulates on seashores driven by the action of currents, wind and tides [3]. Once cast ashore, the seaweed can be washed back into the ocean or stay on the beach. An excess of algae remaining on the beach is considered an environmental problem, because seaweed stockpiles need to be removed before using the littoral for recreation purposes. The harvesting of seaweed collected on the beach for specific commercial uses, as, for example, agar extraction, is not very important. However, this naturally occurring renewable biomass could be valorized as a char feedstock and produce a stable material for soil amelioration [4].

The composition of algae varies between species; typically, protein, lipid and carbohydrate contents range between 6–70%, 2–50%, and 4–64%, respectively [5]. Unlike terrestrial plants, lignin is only present in some red algae [6]. Algae exhibit a higher ash content than lignocellulosic plant biomass, which can vary between 13.1% to 42.8% on a dry basis, with a mean value of 26.6% [1]. In this way, algal-based fertilizers and amendments, including biochar, differ from those based on lignocellulosic materials [7]. Beach-cast seaweeds have been converted to fertilizers, contributing to sustainable development and a circular economy, in different countries of the world [8]. In this way, it has been found that the composting of macroalgae diminishes their volume on seashores [3], but this is a time-consuming process, associated with undesirable environmental impacts, including odor and greenhouse gas emissions [8]. In this scenario, the production of beach-cast seaweed biochars could be a more suitable approach to manage this feedstock, due to the shortened production time (a few hours). On the other hand, biochars prepared from different natural and commercially cultivated algae species have been shown to be efficient in amending soils and in controlling and remediating harmful environmental pollutants. Hence, the use of single algae species as char feedstock yielded a product with several defining characteristics [9–11], with properties suitable for its use as a soil fertilizer [10] but also as part of a waste valorization strategy [8,12].

Beach-cast seaweed is a low-cost abundant feedstock, and therefore it can be employed for applications on a large scale [13]. It should be noted that the harvesting of this material is regulated in many countries and requires licenses, due to its ecological importance. The economic viability of BC production depends not only on the cost of the raw material but also on several other factors, mainly the costs of production technologies [13]. In general, production costs are higher than other costs and are associated with BC's suitability for a given use, according to its physicochemical properties. Therefore, the production of BC from beach-cast seaweed is not expected to be more expensive than that of lignocellulosic biochar, and its fittingness as a cost-effective soil ameliorant presumably depends on its unique physicochemical properties. In fact, it has been stated that macroalgal biochar can serve as a cost-effective fertilizer [13] and a low-cost adsorbent [14].

Pyrolysis temperature and residence time are the main parameters explaining the properties of BCs from different feedstock, including beach-cast seaweed biochars [4]. Thus, the impact of these parameters on the characteristics of BCs from single natural and commercial cultivated algae species has been addressed before; however, not always is this information available [13]. For instance, a seminal study on the characterization of BC derived from seven algae species did not evaluate the influence of pyrolysis parameters, still concluding that BCs could work as a soil ameliorant and improve soil carbon sequestration [4]. Nevertheless, others studied [15–17] the influence of pyrolysis temperature in the properties of algal BCs, focusing on the changes in BC yield, ash content, pH, electrical conductivity, elemental analysis and use for soil phosphate adsorption, implying that the pyrolysis temperature affected biochars' physicochemical properties [15]. In addition, BC from *Cladophora glomerata* was produced at different pyrolysis temperatures (300, 350, 400 and 450 °C) with emphasis on its suitability as a bio sorbent of toxic metals for wastewater treatment [16]. Also, the influence of pyrolysis temperature in algal BCs and their benefits as organic nutrient sources have been addressed before [17]. Moreover, investigations into the use of algal biochar for soil improvement, produced at a single pyrolysis temperature, have been carried out on six commercially cultivated seaweed species [18].

The abovementioned information shows that algal-based biochars, derived from natural and cultivated species, exhibit a fast decomposition rate and high available N, P and K concentrations [12,17]. In addition, reviews on algal BC production and on the use of algae for bio-oil production, bioenergy and bio-syngas are available [13,19,20]. However, until now, very few studies have been conducted focusing on the use of beach-cast seaweed to produce BC. Thus, information about the characterization of BCs derived from this feedstock is scarce. Our literature review found only a study dealing with *Sargassum*

cymosum beach-cast BC pyrolyzed at a single temperature of 800 °C for assessing the adsorption capacity of acetaminophen [21]; the BC of this single beach-cast species was characterized by several physicochemical methods, but elemental and proximate analyses were not performed. In general, the use of biochars from different feedstocks as a soil amendment has been studied for some years [22–24], but algal BCs have been less frequently utilized as soil ameliorants compared to lignocellulosic BCs. Again, the majority of research on marine algae biochar mainly focused on commercial cultivated algae or the waste generated by this algae industry. Moreover, BC derived from beach-cast seaweed has been only characterized for a single species, but not for a mixture of different natural species. The first step to tailor a biochar to a particular type of soil is to characterize its properties. The characterization of biochar plays a key role in understanding the behavior of and changes in the physical and chemical properties of biochar compared to the input material [25].

In Galicia, at the NW of the Iberian Peninsula, the use of algae has shifted through time, from purely traditional agricultural uses to chemical industries, mainly the food and pharma industries, including the extraction of phycocolloids for human nutrition [26]. The use of raw beach-cast marine algae as a fertilizer has been a traditional practice for centuries. More recently, the composting of this material has been undertaken. Such uses can be considered as valuable routes from an economic and environmental point of view. Nonetheless, and in addition to commercial uses, currently, beach-cast seaweed is considered as a waste, which needs to be continuously removed during beach-cleaning operations by territorial authorities.

We used a wide variety of methods to characterize beach-cast seaweed, staying on the beach and consisting of a mixture of species. These methods included proximate analysis, elemental analysis, general properties, total elements content, ashes content and composition, thermogravimetric analysis, specific surface area, Hg porosimetry, surface morphology, X- ray diffraction, FTIR spectroscopy and the composition of water extracts, including C content, UV–Vis and fluorescence spectroscopies. To the best of our knowledge, such a complete depiction had not been accomplished before for algal-based biochar, derived either from single species or from beach-cast seaweed formed by various species. Moreover, until now, beach-cast seaweed BC has not been sufficiently studied, compared with BC obtained from natural or cultivated algae species and with other feedstock such as lignocellulosic materials or animal manure. In addition, our work provides novel information, as new methods have been used to characterize beach-cast seaweed BC, particularly UV–Vis and fluorescence spectroscopies applied for assessing water-extractable organic carbon. Once characterized, an incubation experiment was carried out in order to assess BCs' suitability for acidic soil amelioration. At the end of the incubation, the soil pH and nutrient availability by Mehlich- 3 were evaluated. Based on the above rationale, the objectives of the present study were as follows: (i) to characterize beach-cast seaweed BCs at different temperatures and residence times, as part of a beach-cast seaweed valorization strategy, and (ii) to analyze the effect of these specific BCs on the amelioration of the soil pH and soil nutrient availability of acidic soils.

2. Materials and Methods

2.1. Raw Material

The beach-cast seaweed was sampled on Cesantes beach (latitude: 42°18′18.5123″ N; longitude: 8°37′01.6680″ W), in the municipality of Redondela, Pontevedra (NW Spain). The sample was a mixture of different species, composed of the green alga *Ulva rigida* and some brown algae represented by *Fucus spiralis*, *Pelvetia canaliculate* and *Himanthalia elongata* and the red alga *Gracilaria vermiculophylla*. The most abundant alga was the species *Himanthalia elongata*, followed by *Ulva rigida* and *Fucus spiralis*. Prior to the production of biochars, beach-cast seaweeds were washed thoroughly with distilled water to remove

unknown biomass and inorganic impurities. Then, the beach-cast seaweed was homogenized after grinding. Finally, the feedstock was air-dried for 24 h and then dried in the oven at 60 °C for 48 h.

2.2. Biochar Production

Pyrolysis was performed using a 12-PR/400 series 8B furnace (Hobersal, Barcelona, Spain) with a temperature programmer. For all biochars, 200 g of beach-cast seaweed was placed in a stainless-steel recipient 20 cm in diameter and introduced into the furnace, and the temperature was increased at a rate of 3 °C min^{-1} until the desired pyrolysis temperature was reached. Two temperatures (300 and 600 °C) and two residence times (1 and 3 h) were tested. The beach-cast seaweed and the produced BCs were sieved to 2 mm prior to their characterization.

2.3. General Properties

The general properties of the biochars and beach-cast seaweed were obtained as follows: solid density was measured with a Accupyc 1340 helium pycnometer (Micromeritics, Norcross, Georgia, United States); pH and electrical conductivity (EC) were determined using a micro pH 2000 (Crison, Barcelona, Spain) and a micro 2201 CM conductivimeter (Crison, Spain), respectively, in aqueous suspensions with a ratio of sample–water of 1:250 (*m*/*v*), after 1 h of agitation in a Rotabit and Boxcult 230V agitator (JP Selecta, Barcelona, Spain); cation exchange capacity (CEC) was determined using the method proposed by Ciesielski and Sterckeman [27], which involves a Cohex extractant solution (sample–solution ratio of 0.5:25 *m*/*v*) and the measurement of cobalt in an Analyst 400 Atomic Absorption Spectrophotometer (PerkinElmer, Waltha, Massachusetts, United States). In addition, the easily oxidized organic carbon (C_{oxi}) was determined using the wet oxidation method described by Walkley Black [28].

2.4. Proximate Analysis

The proximate analyses included the following: (i) The moisture content, measured by drying the samples in a DBS-30 halogen moisture analyzer (Kern & Sohn GmbH, Balingen, Germany) operating at 105 °C until a constant sample weight was achieved. (ii) The mobile/volatile matter (VM), determined in a CR-48 furnace (Hobersal, Barcelona, Spain) heated to 900 °C ,where samples were directly placed for 7 min in covered quartz crucibles. Thereafter, they were allowed to cool down to room temperature and were weighed. (iii) The ash contents, determined by introducing the samples into an AAF 11/18 furnace (Carbolite Gero, Derbyshire, United Kingdom) at 900 °C and holding them for 12 h in covered alumina crucibles. The resident matter/fixed carbon (FC) was calculated as described in [25] by the following equation:

$$FC = 100\% - (\%VM + \%Ash) \quad (1)$$

2.5. Elemental Content

The C, H, N and S contents were determined by dry combustion in a FlashEA1112 elemental analyzer equipped with a MAS200 sampler (Thermo-Finnigan, Somerset, New Jersey, United State), and oxygen (O) content was calculated, following [29], with the formula:

$$O = 100\% - (\%C + \%H + \%N + \%S + \%Ash) \quad (2)$$

Then, the higher heating value (HHV) was estimated according to the following equation, as described in [30]:

$$HHV\ (MJ\ kg^{-1}) = 0.3491 \times C + 1.1783 \times H + 0.1005 \times S - 0.1034 \times O - 0.015 \times N - 0.021 \times Ash \quad (3)$$

2.6. Total Element Content and Elemental Composition of Ashes

Total Na, Mg, P, Ca, Mn, Fe, Cu, Zn and K were measured by inductively coupled plasma mass spectrometry (ICP-MS) in an ELEMENT XR (Thermo-Finnigan, Somerset, New Jersey, United States) after sample digestion with 3:1 (*v*/*v*) concentrated HCl/HNO_3 following the USEPA 3051a method [31]. The elemental composition of the ashes of all materials was determined by X-ray fluorescence (XRF), using an S4 PIONEER (Bruker AXS GmbH, Karlsruhe, Germany) wavelength-dispersive X-ray fluorescence spectrometer (WDXRF).

2.7. Thermogravimetric Analyses

The thermogravimetric analysis (TGA) was performed in a STA 449F3 analyzer (Netzsch, Bayern, Germany) coupled with a differential thermal analyzer (DTA). For the TGA, each sample was processed and heated up to 1000 °C at a flux of 60 mL min^{-1} under an N_2 atmosphere.

2.8. Surface Area, Porosimetry and Morphological Structure

Physical properties were determined with the following equipment: The BET surface area (SBET) and pore size distribution were determined from nitrogen sorption isotherms measured using a TriStar II Plus Version 3.00 analyzer (Micromeritics, Norcross, Georgia-United States) equipped with MicroActive 5.01 software. The Hg porosimetry analyses were made with an AutoPore IV Mercury Porosimeter (Micromeritics, Norcross, Georgia, United States) and MicroActive 5.02 software to process data. The pores were classified as micropores (<2 nm), mesopores (2–50 nm) and macropores (>50 nm) [32–34]. Scanning electron micrographs (SEMs) of the biochars were performed in a JSM 6400 microscope (JEOL, Peabody, Massachusetts, United States) with the purpose of exploring morphological alterations in the surface of the material during pyrolysis [35].

2.9. X-Ray Diffraction (XRD) Analysis

An XRD analysis was conducted to identify the crystallographic structures in beach-cast seaweed and biochars [25]. The powder XRD technique was used in a D4 Endeavor diffractometer (Bruker AXS GmbH, Karlsruhe, Germany) with monochromatized CuK radiation of wavelength λ = 0.154 nm, with 40 kV voltage and 50 mA current. The goniometer diameter was 401 mm. The continuous scan mode was followed to collect 2θ data from 10 to 80° in 0.5° steps. The crystalline phases were identified by comparing them with the diffraction patterns of the standard powder XRD cards compiled by the JCPDS-PDF 2.

2.10. FTIR Spectra

The FTIR spectra of beach-cast seaweed and biochars were measured in transmission mode using KBr pellets. One milligram of the material was mixed with 200 mg of potassium bromide (KBr—FTIR grade-Panreac) and ground to a fine homogenized powder in an agate mortar under an IR lamp to reduce the absorption of air humidity by the mixture. After that, the resulting powder was pressed to 2 MPa with a Specac Mini Pellet Press to produce a pellet. The mid-IR spectra of the pellets were measured in a Thermo Scientific is10 FTIR spectrometer (Thermo-Fisher Scientific, Waltham, Massachusetts, United States) in transmission mode, at wavenumbers between 400 and 4000 cm^{-1} with a resolution of 1 cm^{-1}. Three different pellets were prepared from each material. Each sample was scanned 128 times, and the final IR spectrum was the average of these spectra. After obtaining one spectrum, the same pellet was rotated, and the procedure was repeated in order to obtain two spectra from different parts of the pellet.

After collection, a Savitzky–Golay filter was applied in order to remove noise, and baseline and scatter effects were corrected using an Extended Multiplicative Scatter Correction (EMSC) method [36] using the package EMSC in R [37]. The final spectrum for the

raw material and each biochar was the average of 6 corrected spectra (3 pellets × 2 spectra from each pellet).

2.11. Water-Extractable and Dissolved Organic Carbon

The water-extractable organic carbon (WEOC) was measured in aqueous extracts using a sample–water ratio of 1:4 (*m*/*v*), after agitation for 1 h and filtration at 2.5 μm, by means of a combustion and catalytic oxidation and near-infrared spectroscopy (NIRS) determination with a Formacs HT analyzer (Skalar, Breda, The Netherlands). In addition, the dissolved organic carbon (DOC) was measured with the same extraction and equipment used for the WEOC prior filtration through a filter with a pore size of 0.45 μm.

2.12. UV–Visible Absorbance and Fluorescence

The UV–Vis absorbance spectra and fluorescence excitation–emission matrices (EEMs) were measured in WEOC extracts prepared as described in the water-extractable and dissolved organic carbon section. The UV–Vis absorbance of the filtered extracts was measured in a 1 cm quartz cuvette in the 200–1000 nm range in 2 nm increments using a Zuzi UV–Vis 4418 spectrophotometer (Auxilab, Pamplona, Spain). When the absorbance of the samples was above 1.5, the extracts were diluted to ensure that the measurements were conducted in the range of concentrations where the Lambert–Beer law applies [38]. The specific UV absorbance at 254 nm ($SUVA_{254}$ index), commonly used to characterized WEOC, was calculated as the ratio of specific absorbance at 254 nm, divided by the optical path (1 cm) and multiplied by 100.

Fluorescence EEMs were measured in the solid–water extracts or their dilutions using a FluoroMax®—4P spectrofluorometer (Horiba, Kyoto, Japan). The excitation wavelengths were between 220 and 520 nm, and emission was measured at wavelengths between 224 and 700 nm. In both cases, measurements were conducted in 4 nm increments. For each excitation wavelength, emission intensities (S) were corrected against those measured in a reference detector (R) as the ratio S/R, to account for differences in the intensity of the excitation light. Corrections of the EEMs obtained were made following several steps that included the removal of Rayleigh scattering, inner filter effect correction [39] and the subtraction of EEMs of blank samples [40]. The resulting EEMs were expressed in Raman units using a water Raman peak intensity at ex/em 300/397 nm [41]. The total fluorescence of each EEM was calculated as the sum of all emission intensities in the EEMs.

2.13. Soil Characteristics and Biochar Amendments

To study the application of beach-cast seaweed biochar as a soil amendment, two of the fabricated biochars, BA300-1h and BA600-1h, were selected and mixed with two acidic soils. Biochars produced at two different temperatures were sorted out, because they exhibited contrasting properties, while, on the contrary, residence time led to minor differences in biochar properties.

Two agricultural soils were sampled at A Coruña province, Galicia, Northwestern Spain. These soils were developed over contrasting parent materials, namely, Granodiorite and Schist. The former was collected at A Zapateira (43°19′48″ N, 8° 24′37″ W: 65 m asl) and the latter at Anceis (43°16′12″ N, 8°21′28″ W; 90 m asl). Both soils are nutrient-poor acidic and rich-in-organic-matter soils, typical to the Galician region and of large geographic extent, and they are categorized as *Umbrisols* [42] or Inceptisols [43]. The soil developed over Granodiorite was classified as a humic Umbrisol, while the soil developed over Schist was classified as a cambic Umbrisol; hereinafter, they will we referred to as HU and CU. The HU soil was sandy loamy textured, while the CU soil was loamy textured.

An incubation experiment was carried out for 8 weeks. Biochars were added to soils at a 10% rate; thus, for a total mixture of 300 g, 270 g of soil + 30 g of biochar was used. A

control soil was maintained without biochars for each soil (HU and CU). Three treatments were set up: (i) control soil, (ii) soil + BA300 and (iii) soil + BA600. The control soils and the amended soils were sieved through 2 mm meshes. The treatments were maintained in an incubator at 20 °C for four months at a constant weight.

At the end of incubation, the pH and the Mehlich- 3 (M3)-available P, K, Ca, Mg, Fe, Mn, Cu and Zn were measured. pH was determined using the micro pH 2000 (Crison, Spain), quoted before for biochar characterization. Determinations were carried out in aqueous suspensions with a ratio of sample–water of 1:2.5 (*m*/*v*), after 10 min of continuous manual agitation with a glass stirring rod. The available P, K, Ca, Mg, Fe, Mn, Cu and Zn were measured for controls and amended soils after extraction with M3. The M3 solution was prepared with acetic acid (CH_3COOH), ammonium nitrate (NH_4NO_3), ammonium fuoride (NH_4F), nitric acid (HNO_3) and ethylenediaminetetraacetic acid (EDTA) at 2.5 pH [44]. Incubated samples were placed for 20 min with M3 solution in a horizontal shaker, using 5 g of soil in 50 mL of extractant and then filtered. The extract was measured by inductively coupled plasma mass spectrometry (ICP-MS) in an ELEMENT XR (Thermo-Finnigan, United States).

2.14. Statisitcal Analysis

The statistical analyses were performed using Statgraphics Centurion® software Version 19.6.03. A one-way analysis of variance (ANOVA) was used to interpret the results. To perform the ANOVA, the type of material (beach-cast seaweed, BA 300-1h, BA 300-3h, BA-1h and BA-3h) was used for variables measured during characterization, while the type of soil and soil plus biochar mixture (CU, CU + BA 300, CU + BA 600, HU, HU + BA 300, HU + BA 600) were used for variables examined in the course of soil amelioration assessments. After the one-way analysis of variance, a Duncan test was conducted. Mean values were deemed to be significantly different when $p < 0.05$.

3. Results and Discussion

3.1. Basic Properties of Beach-Cast Seaweed and Derived Biochars

Table 1 shows the general properties, elemental content and proximate analyses of the beach-cast seaweed and derived biochars, with all data calculated on a dry basis. The solid density of the beach-cast seaweed was higher than the derived biochars, except in the case of BA600-1h. These results were different from those reported by other investigations carried out with biochars derived from miscanthus grass, mesquite wood and coffee residues, which showed increases in solid density with the pyrolysis temperature [45,46]. These authors related the results with the ash content of samples and H/C and O/C ratios; nevertheless, the ash content in the present data fluctuated between 13.02 and 22.74%.

The pH increased, after thermal treatment of the beach-cast seaweed, with pyrolysis temperature. For BA300, significant differences were found with residence time, with a higher pH value for BA300-3h compared to BA300-1h, but for BA600, the residence time was not relevant for pH. The changes can be attributed to the enrichment in carbonates [47] and ash content [22]. According to Shinogi and Kanri [48], the increase in pH can be explained by the complete separation of organic materials and alkali salts at 300 °C. Likewise, Ronsse et al. [49] observed an increase in pH of materials after pyrolysis and with temperature, but the range of this shift can vary with the algae species used as raw material.

The EC values increased for the produced biochars compared to beach-cast seaweed feedstock, and this was more evident for BA300-1h and BA300-3h. The increase in EC can be attributed to poor graphitization, supported by high values of H/C ratios [50]. In the present study, the data exhibited the same trend, with the highest values of EC and H/C ratios for biochars fabricated at 300 °C, compared to those produced at 600 °C. Generally, in the case of biochars, the EC decreased with the increase in pyrolysis temperature, in agreement with the results of Nanda et al. [51]. The influence of the residence time on EC

was only evident in BA300, with statistical differences between BA300-1h and BA300-3h but not for BA600.

The CEC decreased after pyrolysis, with the lowest values for BA600-1h and BA600-3h compared to the beach-cast seaweed. The same trend was found by Chen et al. [52]. This change could be due to the losses of the oxygen-containing functional group as the result of volatilization [53]. CEC values did not depend on residence time. The easily oxidized carbon (C_{oxi}) was lower for biochars fabricated at 600 °C compared to biochars produced at 300 °C and the beach-cast seaweed. There were no significant differences between the Coxi for biochars at each temperature with varying residence times. The results were related to those carbon structures that are easily oxidized for biochars at low temperatures.

The beach-cast seaweed biochars produced at 600 °C presented VM values below 20%, which were comparatively lower than for biochars at 300 °C and for beach-cast seaweed. The ash content presented the highest values for BA600-1h and BA600-3h, while the lowest value was found in BA300-3h. The FC of the samples followed a trend of Algae < BA300-1h < BA300-3h < BA600-1h < BA600-3h, with an important increase in FC in biochars prepared at 600 °C.

The influence of pyrolysis temperature on biochars' properties (ash, VM and FC) is clear, but in the case of the residence times could not be generalized. The coefficients of variation were lower than 5%, evaluated for the samples at different residence times, in the following cases: (i) VM content in BA300 samples, (ii) ash content in BA600 and (iii) FC content in BA600 samples. The coefficients of variation fluctuated between 5% and 10% for the samples at different residence times in the following cases: ash content in BA300 and VM in BA600 samples. The coefficient of variation was greater than 10% in FC content for BA300 samples with a specific value of 10.79% of the coefficient.

The proximate analyses' VM, ash and FC allowed one to infer the presence of more stable C structures in biochars at 600 °C compared to biochars obtained at 300 °C [27], supported by a high FC and low VM for BA600. The VM, FC and ash content for beach-cast seaweed biochars were evaluated by other authors [13] with values similar to the ones obtained in the present work. The VM according to these authors can fluctuate between 50% and 80%, the FC from 10.6% to 18.2% and the ash content between 3.0% and 29.1%. Therefore, the trends observed in the present research have been previously observed by other authors [49,54].

The total contents of carbon and nitrogen for beach-cast seaweed were lower than for the derived biochars. Among biochars, the C content oscillated between 49.2 and 57.4%, and the variability was low. The hydrogen contents were lower for 600 °C biochars compared to the other materials, but minimal variations (<3% coefficient of variation) were registered according to the residence time. The sulfur contents were low for all biochars and for the beach-cast seaweed feedstock. The oxygen content was significantly higher in beach-cast seaweed (34.4%) compared to the derived biochars. In the latter, values did not exceed 18%, and for biochars at 300 °C, no significant differences were found between the two samples, but for biochars at 600 °C, the percentage was lower for BA600-3h compared to BA600-1h (23.2% coefficient of variation). Therefore, oxygen content decreased after the thermal treatment of the beach-cast seaweed. The atomic ratios H/C, O/C and (O + N)/C showed a similar behavior, with higher values for the beach-cast seaweed compared to the derived biochars.

The percentages of total hydrogen and oxygen in the BA600 samples indicate that high temperatures produces dehydration and decarboxylation reactions, supported by low H/C and O/C ratios [55,56]. In this scenario, the high O/C ratio can suggest the presence of more hydroxyl, carboxylate and carbonyl groups [55] for beach-cast seaweed, with higher values compared to those obtained for BA600-1h and BA600-3h. In general, the changes in biochars' chemical properties were related to pyrolysis temperature. Other au-

thors have stated that pyrolysis temperature and biomass (raw material) have a determinative influence on biochar properties (composition, toxicity and agronomic properties) [57].

Regarding HHV data, the lowest amount was found for beach-cast seaweed. Values increased for the derived biochars, but they did not exceed 16.14 MJ kg^{-1}. These figures were lower than those obtained for agricultural waste biochars [58] at different temperatures (250, 350 and 450 °C), with HHV values ranging from 23.08 to 24 MJ kg^{-1}. Nonetheless, the feedstock of the aforementioned biochar corresponds to lignocelullosic materials (date leaves, ornamental plant residues, grass clippings and coconuts leaves). Comparing the present HHV values with the results obtained by Méndez et al. [12] for hydrochars from macro algae waste, a similar trend was found, with increasing HHV after the thermal process; however, the values were higher, ranging from 18.49 MJ kg^{-1} for the raw material to 23.25 MJ kg^{-1} for hydrochar produced at 230 °C and 6 h of residence time. These differences could be due to the thermal process used to transform the biomass. In the case of hydrothermal carbonization, the working temperatures are lower than in pyrolysis, but the process is performed at a higher pressure.

As stated in the materials and methods section, in our work, a mixture of algae was used (*Ulva rigida*, *Fucus spiralis*, *Pelvetia canaliculata*, *Himanthalia elongata* and *Gracilaria vermiculophylla*). However, the elemental content has some similarities with the results reported by Parsa et al. [59] for *Gracilaria gracilis* and *Cladophora glomerata*, some macro algae used for biocrude production. According to the present work, the HHV data imply an increase in the calorific value of the materials after pyrolysis that can be suitable for the application of beach-cast seaweed biochar. Comparisons among biochars derived from various algae species can have considerable differences, as shown in a study for eight individual algal species [10].

Table 1. General properties, proximate, element content and elemental ratios of beach-cast seaweed and derived biochars. Means with same letter are not significantly different ($p > 0.05$) using Duncan test.

Sample	Beach-cast seaweed	BA300-1h	BA300-3h	BA600-1h	BA600-3h
		General properties			
Solid density (g cm^{-3})	1.79	1.63	1.58	1.90	1.54
pH	7.11 ± 0.21 a	7.67 ± 0.07 b	8.35 ± 0.11 c	9.36 ± 0.06 d	9.56 ± 0.08 d
EC (μS cm^{-1} 20 °C)	24.50 ± 0.36 a	258.67 ± 8.39 d	144.4 ± 7.3 c	58.10 ± 3.21 b	57.23 ± 4.43 b
CEC (cmolc Kg^{-1})	112.11 ± 5 b	95.11 ± 9.19 b	134.99 ± 41.25 b	36.95 ± 2.24 a	27.58 ± 15.34 a
Coxi (%)	32.36 ± 3.82 b	38 ± 1.84 c	41.38 ± 2.32 c	4.43 ± 0.1 a	2.71 ± 0.88 a
		Proximate analysis			
VM (%)	53.81	47.3	45.1	18.9	16.5
Ash (%)	24.500	25.03	22.66	27.98	29.3
FC (%)	21.69	27.67	32.24	53.12	54.12
		Element content			
N (%)	1.84	2.88	3.03	2.46	2.50
C (%)	33.79	49.19	51.37	55.31	57.44
H (%)	4.89	4.07	4.10	1.56	1.50
S (%)	0.57	0.80	0.76	0.53	0.52
O (%)	34.42	18.04	18.08	12.16	8.73
		Elemental ratios			
H/C	1.74	0.99	0.96	0.34	0.31
O/C	0.76	0.28	0.26	0.16	0.11
(O + N)/C	0.81	0.33	0.31	0.20	0.15
HHV (MJ kg^{-1})	8.85	14.85	16.14	14.00	14.75

3.2. Total Elemental Content and Ash Composition

Table 2 presents the total elemental concentration of macronutrients and micronutrients for the beach-cast seaweed and derived biochar samples, while the composition of ashes expressed as oxides is shown as Table S1. The total Ca and Mg showed the highest element concentrations for all the studied samples. The total Ca and total P increased with increasing pyrolysis temperature. The total K concentrations in all materials were lower than 1 g kg^{-1} except in BA300-1h, with 1.16± 0.43 g kg^{-1}. The Mg concentration was highest for BA600-1h, with a value of 28.97 ± 1.25 g kg^{-1}, compared to the rest of the materials, and it increased in biochars compared to beach-cast seaweed feedstock. In the case of Fe, the beach-cast seaweed presented the lowest quantity among the samples, with 2.85 ± 0.11 g kg^{-1}, and this element increased in the derived biochars. The amounts of total Cu and Zn were similar for beach-cast seaweed and biochars obtained at 300 °C, and higher for biochars obtained at 600 °C. Each element had a different trend among the samples, but in general, the pyrolysis temperature plays an important role, while a change in residence time did not result in significant changes; however, this was not the case for Ca, Mg and Zn, because statistical differences between residence times were found for these elements.

There was a noticeable increase in macro element concentrations with the increasing of pyrolysis temperature compared to beach-cast seaweed. These results were consistent with those reported by Michalak et al. [16], with greater values of Ca, Mg, P and K with the increase in pyrolysis temperature. These findings allow to speculate on the possibility of the materials being a nutrient supply for soil and, more generally, resulting in the improvement of crop productivity, particularly in acidic soils [4].

The composition of the ashes determined by and expressed in oxides is shown as Table S1. The concentrations of the main oxides ranked as follows: CaO > MgO > SiO_2 > SO_3 > Al_2O_3. The total element content determined by acidic extraction and ash composition measured by FRX indicate that Ca and Mg were the most abundant elements in the beach-cast seaweeds and their derived biochars. In general, the total elemental contents of the feedstock and biochars increased with increasing ash content, but this was not the case for oxide content in the ashes. For example, CaO contents in the ashes were rather close, ranging from 9.1% to 9.7%, but MgO contents increased with increasing ash content and thus with increasing pyrolysis temperature and residence time. Noteworthily, beach-cast seaweed contained more SiO_2 and Al_2O_3 than the resulting biochars, while SO_3 strongly decreased after combustion at 600 °C; similar trends in oxide concentrations following pyrolysis have been previously observed [1].

The higher ash content commonly present in seaweed compared to terrestrial plants is consistent with the accumulation of inorganic substances as mineral depots, which has been verified in many algae species. Both inorganic non-crystalline and crystalline forms may be present in natural conditions. In addition, low quantities of sand particles and mussel debris might be found as impurities and eventually contribute to increase the ash content.

Calcification, i.e., the crystallization of calcite, is the most common process of mineral incorporation into seaweed [1,7,60]. Part of the calcite might be transformed later into calcium hydroxide. Thus, the highest contents of total Ca and CaO obtained in this study are compatible with algae calcification. This notwithstanding, mussel debris could also contribute to increase CaO content.

Biogenic silica may also be present in algae and their ashes, as a non-crystalline form [1]. In addition, the contribution of silica or silicates to ashes may result from several potential types of contamination, for example, by the deposition of sediments or diatoms (microalgae with a silica wall) on the debris, which has been evidenced in the SEM images of the sample BA300-1h (Figure S1). Moreover, the observation that, with increasing temperature and ash content in biochars from beach-cast seaweed, less silica was measured by XRF, may be explained by an increase in the semi-crystalline or non-crystalline phases of SiO_2 during pyrolysis, which are not measured using this technique [60].

In addition, amorphous or semi-crystalline phases of substances containing MgO, SO_3, P_2O_5, K_2O, etc., and other oxides measured in the ashes could be formed during the pyrolysis process, but the resulting mineral phase was not identified due to the low resolution of the XRD.

Table 2. Total elements content (g kg^{-1}) for beach-cast seaweed and derived biochar samples. Means with same letter are not significantly different ($p > 0.05$) using Duncan test.

	Beach-Cast Seaweed	BA300-1h	BA300-3h	BA600-1h	BA600-3h
P	1.55 ± 0.09 a	1.82 ± 0.02 b	1.95 ± 0.07 b	3.16 ± 0.13 c	3.33 ± 0.15 c
K	0.27 ± 0.01 a	1.16 ± 0.43 c	0.87 ± 0.03 b,c	0.75 ± 0.07 b	0.72 ± 0.03 b
Ca	36.56 ± 3.75 a	45.6 ± 0.31 b	43.73 ± 4.13 b	65.49 ± 4.2 6 d	58.58 ± 2.76 c
Mg	10.52 ± 0.72 a	19.52 ± 0.19 b	20.21 ± 0.65 b	28.97 ± 1.25 d	24.44 ± 0.89 c
Fe	2.85 ± 0.11 a	3.61 ± 0.06 b	3.7 ± 0.15 b	4.58 ± 0.21 c	4.46 ± 0.13 c
Mn	0.14 ± 0.01 a	0.22 ± 0.02 b	0.2 ± 0.02 b	0.27 ± 0.02 c	0.27 ± 0.02 c
Cu	0.02 ± 0.001 a	0.02 ± 0.001 a	0.02 ± 0.001 a	0.03 ± 0.003 b	0.03 ± 0.001 b
Zn	0.13 ± 0.01 a	0.11 ± 0 a	0.11 ± 0.01 a	0.18 ± 0.01 b	0.23 ± 0.02 c

3.3. Thermogravimetric Analysis (TG)

Figure 1 represents the TG curves of the beach-cast seaweed and derived biochars. The beach-cast seaweed showed a first mass loss of 5.05% between 22–200 °C. After this point and up to a temperature of 570 °C, the second mass loss was identified, showing the highest percentage, with a value of 44.48%. Finally, two subsequent small mass losses of 4.74% and 3.61% were recognized at about 740 °C and 1000 °C, respectively. For the sample BA300-1h, the first mass loss ended around 200 °C, with a 1.94% mass loss. Then a 35.59% mass loss was observed until 625 °C, and a continuous weight loss of 10.23% was identified until the highest temperature plotted. The data for the BA300-3h sample showed a significant mass loss of 31.70% between 200 °C and 600 °C. At the initial temperature until 200 °C, the percentage of loss was 1.78%, and after 600 °C until 1000 °C, it was 11.42%. The changes in mass for biochars obtained at 600 °C displayed only two mass loss zones; the first one corresponded to the initial temperature until 330 °C, with 1.28% and 1.96% for BA600-1h and BA600-3h, respectively. In the range of >330 °C to around 1000 °C, the mass loss percentages were 18.13% for BA600-1h and 14.70% for BA600-3h.

Figure 2 denotes the DTA curves, with three noticeable zones for the beach-cast seaweed; the first corresponds to 0.86% min^{-1} at 112.3 °C, the second to 3.29% min^{-1} at 334.4 °C and the last one to 0.42% min^{-1} at 681.6 °C. For BA300-1h, the three zones of DTA were −0.42% min^{-1}, −1.76% min^{-1} and −0.65% min^{-1} at the following temperatures 99.9 °C, 422.5 °C and 693.6 °C, respectively. For BA300-3h, the DTA exhibited the following peaks: −0.36% min^{-1} at 105.3 °C, −1.82% min^{-1} at 443.7 °C and −0.70% min^{-1} at 695.3 °C. For BA600-1 h, the first point was −0.22% min^{-1} at 103.5 °C and the second one was −0.55% min^{-1} at 689.5 °C. For BA600-3h, the first point was −0.21% min^{-1} at 102.4 °C and the second one was −0.59% min^{-1} at 699.5 °C.

The thermogravimetric analysis allowed conclusions to be drawn about the thermal stability of the samples. According to the TG and DTA graphics, the more stable material is the biochar pyrolyzed at 600 °C, with only two relatively small zones of weight loss. This was supported by the results obtained in the elemental and proximate analysis and the low H/C ratios, in agreement with the data found by other authors [61].

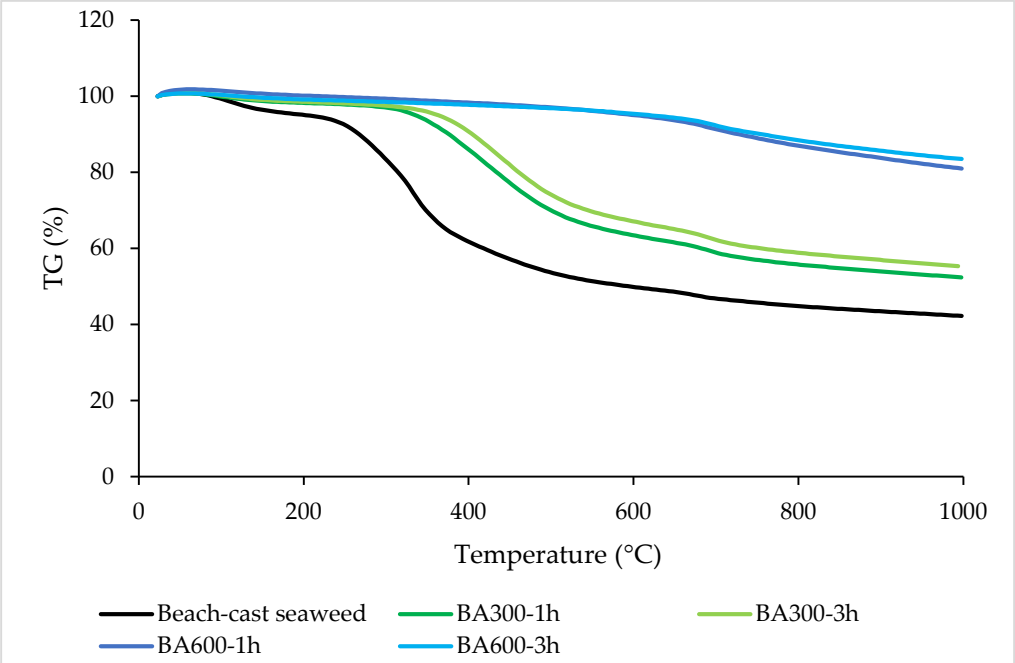

Figure 1. TG curves for the beach-cast seaweed and the derived biochars samples: BA300-1h, BA300-3h, BA600-1h and BA600-3h.

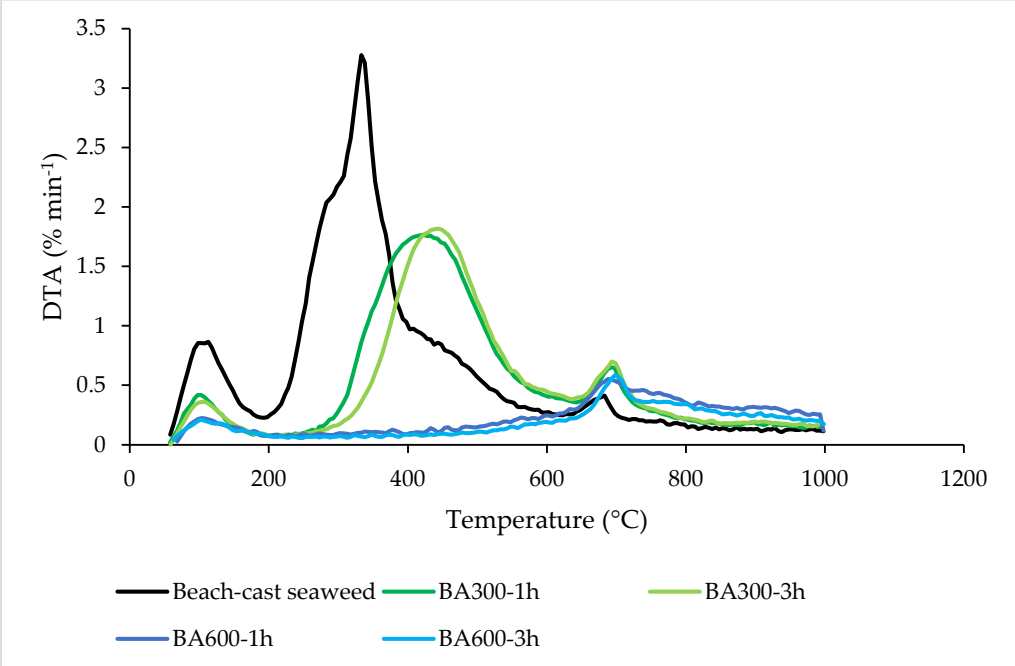

Figure 2. Differential thermal analysis (DTA) curves for the beach-cast seaweed and the derived biochars samples: BA300-1h, BA300-3h, BA600-1h and BA600-3h.

3.4. Porosity and Surface Area

Table 3 shows the S_{BET}, porosity and pore volume for the beach-cast seaweed and the derived biochars. The S_{BET} increased slightly after pyrolysis, and the highest values were the ones of biochar at 600 °C, but no differences were found between residence times at this temperature. In general, the values for S_{BET} were lower than 2 m^2 g^{-1}. The porosity of samples varied between 44.81% and 54.77% with the lowest value for BA300-3h and the highest for the beach-cast seaweed. The micropore volumes were below the detection limit, while the mesopore volumes were low, compared to the macropores volume. Figure

S2 represents the cumulative pore volume for all samples related to the pore size diameter, where the beach-cast seaweed presented a higher pore volume than the biochars. In addition, the morphology exhibited in the SEM images (Figure S3) can support the data obtained in the surface and porosimetry analyses, with a less microporous surface.

The surface area of biochars at 300 °C did not change compared to the beach-cast seaweed, but for biochars at 600 °C, the values increased, indicating the important role of pyrolysis temperature in this physical characteristic. The same trend was found for eight biochars from different algae species [4], with a change from 1.15 $m^2\ g^{-1}$ at 305 °C to 4.26 $m^2\ g^{-1}$ at 512 °C.

The use of biochar as a soil amendment due to its porous structure and high surface area is well known, and the presence of macropores might be useful for soil microbiota [34].

Table 3. S_{BET}, porosity and pore volume of mesopores (V meso) and macropores (V macro) for beach-cast seaweed and derived biochar samples.

Sample	SBET ($m^2\ g^{-1}$)	Porosity (%)	V meso ($cm^3\ g^{-1}$)	V macro ($cm^3\ g^{-1}$)
Beach-cast seaweed	0.892	54.77	0.04	0.74
BA300-1h	0.9569	45.89	0.04	0.48
BA300-3h	0.9886	44.76	0.03	0.48
BA600-1h	2.0444	51.71	0.07	0.55
BA600-3h	2.1869	44.81	0.06	0.41

3.5. X-Ray Diffraction

XRD difractograms from the beach-cast seaweed and the derived biochars (Figure 3) showed, on the one hand, broad humps, which indicated the amorphous and semi- or pseudo-crystalline nature of organic structures and, on the other hand, sharp peaks, which reflect the presence of inorganic minerals.

All the samples studied present a quartz peak at about 2θ = 26.7°. However, the intensity of this peak is much higher in the feedstock and in biochar produced at 600 °C than in biochar at 300 °C. Nevertheless, the presence of crystalline SiO_2 in sample BA300-1h is proved by salient peaks at 2θ = 67.8° and 2θ = 68.3° (overlapping with a calcite peak); similarly crystalline SiO_2 in sample BA300-3h is evidenced by a sharp peak at 2θ = 59.9° and other minor peaks along the difractogram. Calcite peaks at 2θ = 29.5° and in other positions with moderate to low intensities were found in all the studied samples. In addition, crystalline calcium hydroxide (portlandite) also was observed, frequently overlapping calcite peaks; this phase could be newly formed from the hydroxylation of lime by sea water or even air moisture during accumulation at the shore or storage, respectively [1].

In summary, it was found that calcite, quartz and pentlandite were the major predominant crystalline phases. The dominance of these inorganic minerals associated with the sharpest XRD peaks is consistent with the higher contents of CaO, and MgO, SiO_2 in the ashes (Table S1). In addition, a few crystalline and semi-crystalline phases in the derived biochars close to the XRD detection limit belonging to minerals with P, Na, Mg and Al have been detected.

Also, the XRD showed the formation of highly ordered aromatic structures, with increasing pyrolysis temperature. The amorphous structure of the beach-cast seaweed difractogram, with a broad hump at 2θ from about 12° to 25°, is compatible with hydrated proteinaceous and carbohydrate materials. Notably, increasing pyrolysis temperatures resulted in broad peaks at the 2θ values of around 23° and 43° that indicated the development of atomic order in the increasingly carbonized material. The diffraction patterns at 300 °C indicate the presence of amorphous and semi-crystalline cellulose. With an increasing pyrolysis temperature at 600 °C, some partial crystalline structures of cellulose has

been lost. Notwithstanding the diffraction pattern of the sample, BA600-3h showed the presence of crystalline graphite.

In the crystalline phases, the presence of calcite and portlandite were consistent with the previous findings of algae calcification [62,63] and hydroxylation, respectively. In addition, the crystalline SiO_2 in the beach-cast seaweed is of biogenic origin, even if some silicate impurities, resulting from the incomplete washing of mineral particles, should not be excluded. Altogether, the XRF analysis of ashes and XRD support the hypothesis that most of the ashes in the beach-cast seaweed do not originate from contamination but have a biogenic origin.

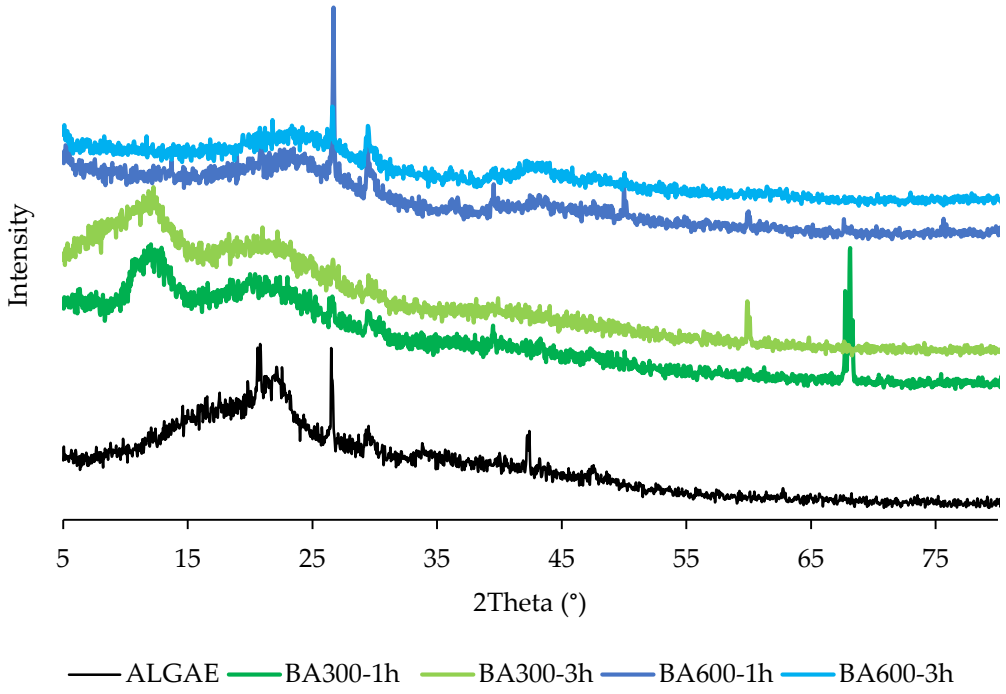

Figure 3. X-ray diffraction analysis (XRD) for the beach-cast seaweed (algae) and the derived biochar samples.

3.6. FTIR Spectra

The FTIR spectra of the beach-cast seaweed and the derived biochars obtained with two pyrolysis temperatures and two residence times are presented in Figure 4. The most relevant changes in functional groups were dependent on the temperature of the pyrolysis, while the residence time had a minor effect. Changes in FTIR spectra with pyrolysis treatment included a decrease in the contribution of regions 3100–3600 and 1500–1700 cm^{-1} to the spectra, which are associated with free –OH groups, including water. This change is more evident at 600 °C. Thus, increasing the temperature led to the dehydration of beach-cast seaweed, but also to a progressive decrease in surface -OH functional groups. In addition, pyrolysis led to the disappearance of the peaks at 1329, 1266 and 985 cm^{-1}, associated with cellulose [64], and 1053 cm^{-1}, which is assigned to the C-O-C and C-OH functional groups, related to the presence of polysaccharides, phenols and esters [65]. The peak at 1157 cm^{-1}, which also disappeared at the lowest pyrolysis temperature, is related to the presence of the C-O of carbohydrate rings [66]. The removal of these peaks occurred at the lowest temperature and residence time, indicating the thermal transformation of polysaccharides in the beach-cast seaweed. Other changes include the decrease in the intensity of the peak at 1643 cm^{-1}, which is usually assigned to C=O carboxyl and amides

[67], and that at 1594 cm^{-1}, related to asymmetric carboxylic stretching [68]. These changes occur mainly at the highest temperature. Bands at 2958, 2917 and 1376 cm^{-1} indicate the presence of aliphatic C-H functional groups [69,70]. Changes in these functional groups were observed only at a temperature of 600 °C, with a residence time of 1 h.

Concomitant to the decrease in the intensity of these bands, other ones become more prominent after pyrolysis. These include the bands at 1422 cm^{-1}, related to aromatic C=C bonds, at 1376 cm^{-1}, commonly assigned to aliphatic C-H [70], and at 872 cm^{-1}, which is indicative of the presence of C-H and C=C functional groups in aromatic compounds [71].

Based on these observations, it seems that pyrolysis produced the breakdown of polysaccharides, which occurs at the lowest temperature, and a progressive removal of O-containing functional groups (OH and carboxyl), which occurs at different temperatures, depending on their nature. At a temperature of 300 °C, some features from the beach-cast seaweed are still present, like the presence of OH and carboxyl peaks. Concomitant to the removal of O-containing functional groups, an increase in the importance of aromatic structures and C-H functional groups can be observed.

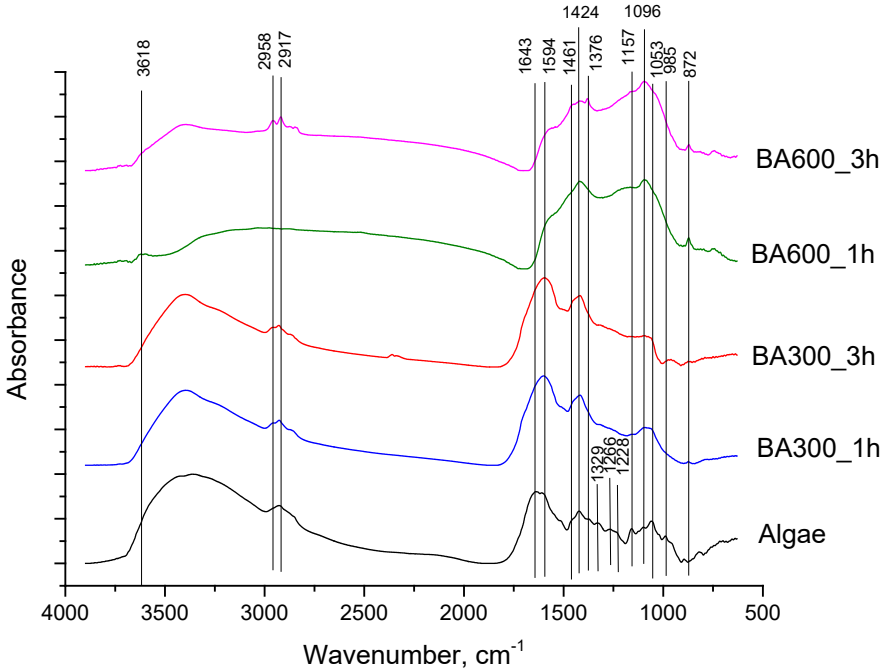

Figure 4. Fourier transform infrared spectra of the beach-cast seaweed (algae) and the derived biochar samples.

3.7. Soluble Organic Carbon, UV Absorbance and Fluorescence

The production of biochar at 300 °C led to a very high increase in both WEOC (filtered at 2.5 µm), which includes particulate and colloidal matter, and DOC (filtered at 0.45 µm), with respect to the feedstock (Table 4). This increase is probably a result of the cracking of large biomolecules, including polysaccharides, on the cell walls and algae tissues that release smaller compounds. However, when pyrolysis was performed at 600 °C, the amount of WEOC and DOC dramatically decreased to values below those of the original beach-cast seaweed. At both temperatures, residence time had a minor effect on the amounts of WEOC and DOC released, with a slight reduction when increasing it from 1 to 3 h. Regarding DOC, similar results, with high values for biochars produced at lower temperatures compared to those produced at high temperatures, were found by other authors [72,73].

Changes in C extractability was accompanied by changes in WEOC composition, as indicated by the optical properties of the extracts. The $SUVA_{254}$ of the extracts increased

with pyrolysis at 300 °C. This parameter is commonly related to the presence of aromatic compounds in WEOC [74], and thus it should be assumed that OM transformations resulted in a larger proportion of aromatic compounds compared to aliphatic ones in the WEOC of these biochars. Once again, biochar formation at the highest temperature apparently reduced the proportion of aromatic compounds in WEOC, as compared with both the original material and the biochar produced at 300 °C. Since pyrolysis at 600 °C resulted in the lowest WEOC and DOC concentrations, the decline in $SUVA_{254}$ suggests that concentrations of hydrophilic water-soluble aromatic compounds decreased to a higher degree than aliphatic water-soluble compounds. Reactions at high temperatures seem to include condensation/polymerization processes, besides a more intense oxidation of OM, that lead to the formation of polymerized larger-size aromatic compounds that resist extraction by water, thus leading to water extracts showing lower aromatic fractions and higher proportions of aliphatic compounds [75,76].

Total fluorescence, normalized to DOC, revealed that heating at 300 °C produced water extracts with less fluorescent material as compared to the original material (Table 4). According to these results, even though pyrolysis at this temperature produced a larger amount of soluble organic compounds than beach-cast seaweed, these seem to include a lower proportion of fluorescent material than the feedstock. This phenomenon is more pronounced with an increasing heating temperature.

Table 4. Water-extractable organic carbon (WEOC), dissolved organic carbon (DOC), specific absorbance at 254 nm ($SUVA_{254}$) and ratio between total fluorescence and DOC of beach-cast seaweed and derived biochar samples.

	WEOC (<2.5 μm) **mg L^{-1}**	**DOC (<0.45 μm)** **mg L^{-1}**	**$SUVA_{254}$** **cm^{-1}**	**Fluorescence/DOC** **cm^{-1} mg^{-1} L**
Beach-cast seaweed	17.21	8.99	0.07	5074.60
BA300-1h	1478.64	1217.56	0.13	2403.73
BA300-3h	1207.46	823.31	0.14	2778.24
BA600-1h	3.98	3.38	0.02	509.25
BA600-3h	3.23	3.13	0.01	653.81

Excitation–emission matrices of the water extracts obtained for the five materials are presented in Figure 5. Significant changes in the location of the fluorescence peaks are evident among the treatments. Once again, the main changes were observed with the pyrolysis and variations in its temperature, while the residence time had minor effects. The raw material showed a peak at Ex 272/Em 348 nm, which is caused by tryptophan and is indicative of the presence of proteinaceous material. This peak disappeared in all biochars, indicating that pyrolysis produced a breakdown of proteinaceous materials. Heating also produced changes in the relative intensities of peaks at 241/450 and 314/430 nm, which are related to fulvic-like and humic-like materials, respectively [77].

In the extracts of the beach-cast seaweed, the intensity of the peak with shorter excitation wavelengths was larger than the one with longer excitation wavelengths. However, this situation is reversed after pyrolyzing the beach-cast seaweed at 300 °C, where we can observe a larger intensity of the red-shifted peak compared to the blue-shifted one. The pyrolysis at 600 °C once again reverses the situation. Thus, it seems that pyrolysis at 300 °C produces water extracts with more soluble compounds, more aromatic, less fluorescent, than the beach-cast seaweed. These fluorescent components are enriched in humic-like compounds, with a larger molecular weight. An increase in the treatment temperature to 600 °C produced less soluble organic material, less aromatic, less fluorescent, and with more fulvic-like material (with a smaller molecular weight) than the other treatments. These results are consistent with the presence of less aromatic structures in the biochars produced at 300 °C compared to those produced at 600°C. Thus, the higher the aromatic

structures and recalcitrance of the beach-cast seaweed-derived biochars, the lower they are in their respective water extracts.

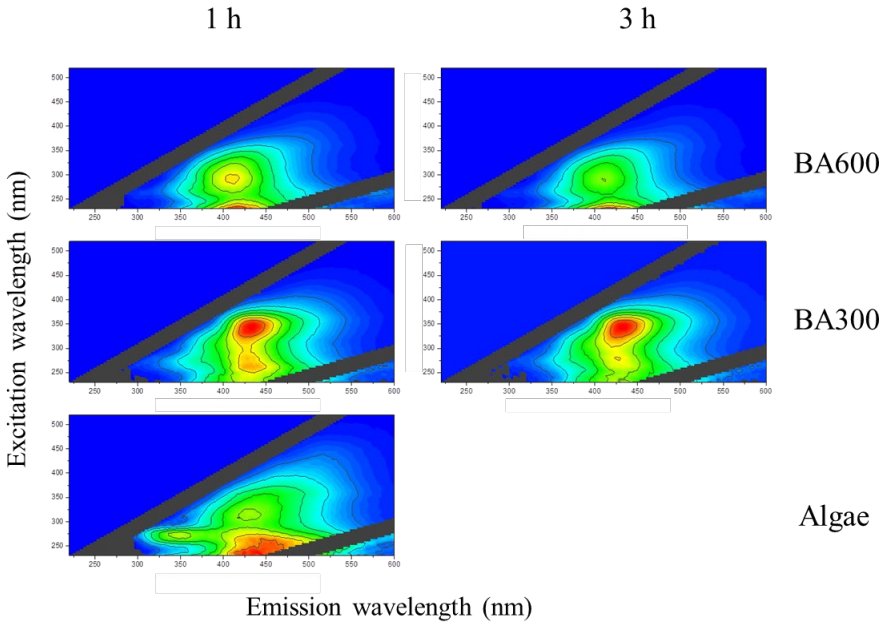

Figure 5. Fluorescence excitation–emission matrices of the water extracts of the beach-cast seaweed (Algae) and the derived biochar samples.

3.8. Effect of Beach-Cast Seaweed-Derived Biochars Addition in Two Acidic Soils

The soil initial pH was 5.47 ± 0.09 for the cambic Umbrisol (CU) and 4.98 ± 0.05 for the humic Umbrisol (HU). Therefore, the former soil is characterized as strongly acid and the latter as very strongly acid; significant differences ($p < 0.05$) were found between the pH of the two studied soils (Figure 6). The biochar pH increased with increasing pyrolysis temperature; it was 7.67 ± 0.07, i.e., slightly alkaline for BA300-1h, and it was 9.36 ± 0.06, i.e., very strongly alkaline, for BA600-1h.

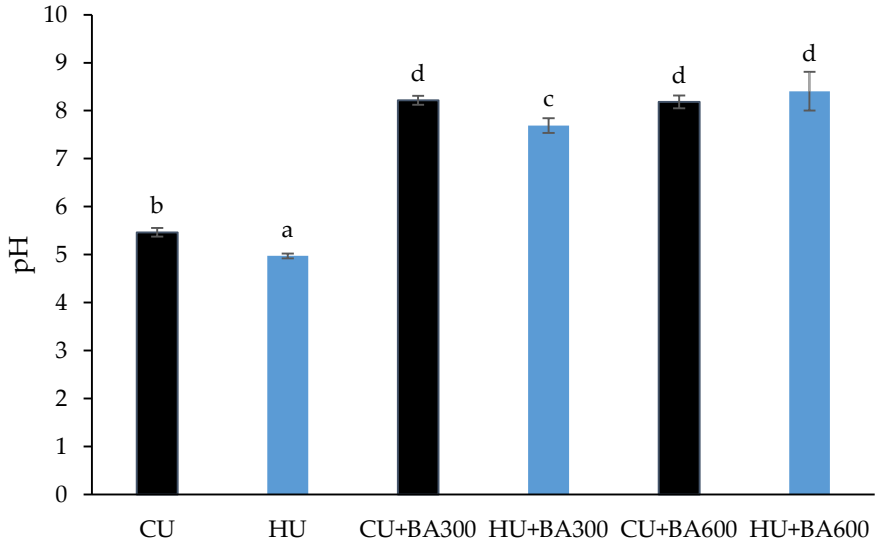

Figure 6. pH values of control soils and soils amended with beach-cast seaweed biochars. The black bars correspond to CU treatments and blue bars correspond to HU treatments.

The soil pH showed consistently positive responses to biochar amendment (Figure 6); overall, very significant differences ($p < 0.001$) were found between the initial soil pH, i.e., the control soil, and the biochar-amended soils, consistent with results from other authors [78,79]. Biochar pyrolysis temperature did not show significant effects in the pH of the amended CU soil; however, pyrolysis temperature significantly ($p < 0.05$) influenced the pH of the amended HU. Application of biochar produced at 300 °C resulted in a slightly alkaline pH of the HU soil; on the other hand, application of biochar produced at 600 °C to the HU soil and that of biochar produced at 300° C and 600° C to the CU soil resulted in moderately alkaline pHs. Moreover, the relative pH increases of the amended soils, relative to the control soil, were higher in the HU soil (54.42% and 68.88% for BA300 and BA 600, respectively) than in the CU soil (50.27% and 49.73% for BA 300 and BA 600, respectively). The higher response of soil pH in the HU soil than that of the CU soil is consistent with the coarser texture and lower initial pH [78] of the former compared to the latter. Soil pH increases after biochar application are related to biochar alkaline characteristics; biochar contains Ca, Mg, K and Na (Table 2), likely in the form of oxides and carbonates (Table S1); these become alkaline after dissolution in water, allowing the neutralization of soil acidity [79,80].

Extractable M3 macronutrient, i.e., P, K, Ca and Mg, concentrations very significantly ($p< 0.001$) increased with biochar addition, both in the CU and the HU soils (Table 5). Regardless of soil type, the available concentrations of these macronutrients were highest for biochar produced at 300 °C than for the 600 °C counterpart. Thus, results for M3-available K, Ca and Mg are consistent with the greater CEC of biochar pyrolyzed at 300 °C than that of biochar pyrolyzed at 600 °C (Table 1).

Comparison of Tables 2 and 5 shows that the response of macronutrientstotal contents of biochar and available contents of soil plus biochar mixtures to the pyrolysis temperature is opposite; this suggests that macronutrient availability is associated to soluble but not to total fractions.

Table 5. Available element (P, K, Ca, Mg, Fe, Mn, Cu and Zn) in mg kg^{-1} content in control soil and soils amended with beach-cast seaweed biochars. Means with same letter are not significantly different ($p > 0.05$) using Duncan test for CU (lower case) and HU (upper case) soils independently.

	CU	CU+BA300	CU+BA600	HU	HU+BA300	HU+BA600
P	77.57 ± 5.46 a	227.98 ± 18.29 c	143.24 ± 4.39 b	141.55 ± 6.85 A	256.23 ± 11.27 C	187.4 ± 9.2 B
K	308.67 ± 6.72 a	451.05 ± 8.2 c	402.37 ± 1.26 b	164.14 ± 6.87 A	264.54 ± 9.86 C	202.81 ± 17.52 B
Ca	276.49 ± 4.74 a	3986.77 ± 53.72 c	1440.85 ± 25.35 b	714.38 ± 22.1 A	4224.46 ± 120.87 C	2845.27 ± 91.7 B
Mg	61.6 ± 7.13 a	2073.73 ± 39.44 c	317.37 ± 2.65 b	122.67 ± 3 A	2096.59 ± 87.33 C	650.11 ± 34.97 B
Fe	385.1 ± 36.44 b	347.49 ± 21.65 b	204.2 ± 13.47 a	257.47 ± 9.97 A,B	317.72 ± 21.39 B	183.35 ± 66.29 A
Mn	122.43 ± 7.14 b	148.7 ± 3.69 c	54.94 ± 3.17 a	26.85 ± 2.87 A	131.77 ± 4.44 B	29.81 ± 4.8 A
Cu	1.49 ± 0.01 a	1.56 ± 0.09 a	2.12 ± 0.09 b	3.97 ± 0.15 A	3.59 ± 0.13 A	4.08 ± 1.29 A
Zn	2.35 ± 0.08 a	10.87 ± 0.4 b	11.28 ± 0.39 b	8.98 ± 0.38 A	18.68 ± 0.01 B	11.53 ± 3.22 A

In general, beach-cast seaweed biochars are rich in macronutrients compared to biochars produced from lignocellulosic feedstocks. In particular, the former feedstock yield biochars with lower C contents but higher available macronutrients and exchangeable cations than the latter. For example, it has been reported that seaweed biochars had high

concentrations of N, P and K [12,13,19]. Similarly, high N, P, Ca and Mg contents in algae species have been proven [23]. Compared to these previous results, in our case study, N, P, Ca and Mg total concentrations and ash concentrations (Tables 1 and 2 and Table S1, respectively) can be considered high, while K concentrations are relatively low.

The relative increases in macronutrient concentrations were higher for the CU than for the HU soil and for the algal biochar produced at 300 °C than for the counterpart at 600 °C. Differences between soils could be linked to initial soil pH. Regardless of soil type and pyrolysis temperature, relative increases in macronutrients ranked as Mg > Ca > P > K.

Changes in micronutrient concentrations after biochar addition did not show a common pattern. In the CU soil, amendment with biochar pyrolyzed at 300 °C increased available Fe, Mn and Zn concentrations and had no effect on Cu concentrations; on the other hand, amendment with biochar pyrolyzed at 600 °C decreased available Fe and Mn and increased available Cu and Zn concentrations. In HU soil, no effects of biochar addition were found on Cu concentrations, irrespective of the pyrolysis temperature; on the other hand, Mn and Zn concentrations were significantly higher after the addition of biochar produced at 300 °C than at 600 °C, while there was no significant effect of biochar additions on Fe concentrations. Soil type, pyrolysis temperature and pH are the main factors affecting increase or reduction in micronutrient availability.

The addition of beach-cast seaweed biochars to soils can be highly effective in ameliorating agricultural soils and improving soil fertility. Algae are rich in nutrients, which in turn are concentrated in the resulting biochars. Beach-cast seaweed biochars increase soil pH and nutrient levels. Moreover, the utilization of these biochars can reduce the demand for chemical fertilizers, providing environmental benefits. Our results also suggest that ameliorating soil chemical properties by biochar amendment depends not only on biochar characteristics, but also on soil properties, especially soil pH, and soil texture. Thus, improving soil fertility by biochar addition requires that local soil factors should be considered.

4. Conclusions

The results obtained by thermogravimetric analysis, elemental analysis and proximate analysis show an important trend indicating that the beach-cast seaweed biochars fabricated at 600 °C were more stable materials. This can be attributed to the presence of organic aromatic compounds. The opposite occurred in the $SUVA_{254}$ of the water extracts, a parameter related to the presence of aromatic compounds, where the data values were higher for biochars fabricated at 300 °C. These results imply that at a high pyrolysis temperature, the changes were due to the formation of polymerized larger-size aromatic compounds that resist extraction by water and resulted in low $SUVA_{254}$, WEOC and DOC values for biochars produced at 600 °C. Therefore, in the studied case, the use of fluorescence, a novel technique for the characterization of algal biochars, confirms the presence of more soluble and more aromatic compounds at 300 °C than at 600 °C.

Regarding the influence of pyrolysis parameters such as temperature and residence time, it was clearly shown that the residence time led to minor differences when compared to temperature in the properties of beach-cast seaweed biochars.

As a general trend, the presence of inorganic materials in beach-cast seaweed and the derived biochars could be related either with the feedstock (biogenic source) or with external impurities. The information provided by XRF and XRD suggest that most inorganic materials identified on beach-cast seaweed and the derived biochars are of biogenic origin. However, detrital materials, including diatoms, mussel debris and sand or clay grains could be present, despite the diligent washing of the original feedstock.

The pyrolysis of beach-cast seaweed led to a carbonaceous material that may be useful as a soil amendment due to its high macro elements content. A soil amendment experiment showed that after 8 weeks, the pH of acidic soils increased to alkaline levels. Moreover, the increase in alkalinity degree depended on the soil type. Biochar addition also

increased M3-extractable macronutrients (P, K, Ca and Mg), suggesting soil fertility improvement in the acidic soils amended with beach-cast seaweed biochars; regardless of soil type, the concentrations of these macronutrients were highest for biochar produced at 300 °C than for the 600 °C counterpart.

In addition, beach-cast seaweed biochars can be a suitable strategy for waste valorization. However, this approach needs to be completed with a life cycle analysis of the biochars that includes the economic perspective.

Overall, this study suggests that the use of biochar derived from beach-cast seaweed as a soil amendment can deliver substantial nutrient benefits to soils and possible improvements in crop productivity, but that there is a need to scale this up, not only in laboratory trials, but also under field conditions.

Supplementary Materials: The following supporting information can be downloaded at: https://www.mdpi.com/article/10.3390/land13060881/s1. Table S1. Composition of ashes (% oxides) of beach-cast seaweed (algae) and the derived biochars samples. Figure S1. Scanning electron microscopy (SEM) of BA300-1h at 1000X. Figure S2. Cumulative pore volume for beach-cast seaweed (algae) and the derived biochars samples. Figure S3. Scanning electron microscopy (SEM).

Author Contributions: Conceptualization, E.C.-A. and A.P.-G.; methodology, E.C.-A., M.L. and A.P.-G.; formal analysis, E.C.-A., G.G., M.L., A.M., J.P.-F. and E.C.-A.; investigation, E.C.-A., G.G., M.L., A.M., J.P.-F. and E.C.-A.; resources, E.C.-A. and A.P.-G.; data curation, E.C.-A. and M.L.; writing—original draft preparation, E.C.-A. and M.L.; writing—review and editing, E.C.-A., G.G., M.L., A.M., J.P.-F. and Paz-González; visualization, E.C.-A., G.G., M.L., A.M., J.P.-F. and E.C.-A.; supervision, A.M. and A.P.-G.; project administration, A.P.-G.; funding acquisition, E.C.-A. and A.P.-G. All authors have read and agreed to the published version of the manuscript.

Funding: This work was funded by the Unión Europea-NextGenerationEU [Grant number UP2021-035, 2022], Ministerio de Universidades and Universidad Politécnica de Madrid.

Data Availability Statement: The raw data supporting the conclusions of this article will be made available by the authors on request.

Acknowledgments: The authors want to thank Xiana Raposo Díaz for her valuable help in the laboratory.

Conflicts of Interest: The authors declare no conflicts of interest.

References

1. Vassilev, S.V.; Vassileva, C.G. Composition, Properties and Challenges of Algae Biomass for Biofuel Application: An Overview. *Fuel* **2016**, *181*, 1–33. https://doi.org/10.1016/j.fuel.2016.04.106.
2. Han, W.; Clarke, W.; Pratt, S. Composting of Waste Algae: A Review. *Waste Manag.* **2014**, *34*, 1148–1155. https://doi.org/10.1016/j.wasman.2014.01.019.
3. López-Mosquera, M.E.; Fernández-Lema, E.; Villares, R.; Corral, R.; Alonso, B.; Blanco, C. Composting Fish Waste and Seaweed to Produce a Fertilizer for Use in Organic Agriculture. *Procedia Environ. Sci.* **2011**, *9*, 113–117. https://doi.org/10.1016/j.proenv.2011.11.018.
4. Bird, M.I.; Wurster, C.M.; de Paula Silva, P.H.; Bass, A.M.; de Nys, R. Algal Biochar—Production and Properties. *Bioresour. Technol.* **2011**, *102*, 1886–1891. https://doi.org/10.1016/j.biortech.2010.07.106.
5. Di Chen, Y.; Liu, F.; Ren, N.Q.; Ho, S.H. Revolutions in Algal Biochar for Different Applications: State-of-the-Art Techniques and Future Scenarios. *Chin. Chem. Lett.* **2020**, *31*, 2591–2602. https://doi.org/10.1016/j.cclet.2020.08.019.
6. Yao, T.; Feng, K.; Xie, M.; Barros, J.; Tschaplinski, T.J.; Tuskan, G.A.; Muchero, W.; Chen, J.G. Phylogenetic Occurrence of the Phenylpropanoid Pathway and Lignin Biosynthesis in Plants. *Front. Plant Sci.* **2021**, *12*, 704697. https://doi.org/10.3389/fpls.2021.704697.
7. Yu, K.L.; Lau, B.F.; Show, P.L.; Ong, H.C.; Ling, T.C.; Chen, W.H.; Ng, E.P.; Chang, J.S. Recent Developments on Algal Biochar Production and Characterization. *Bioresour. Technol.* **2017**, *246*, 2–11. https://doi.org/10.1016/j.biortech.2017.08.009.
8. Harb, T.B.; Chow, F. An Overview of Beach-Cast Seaweeds: Potential and Opportunities for the Valorization of Underused Waste Biomass. *Algal Res.* **2022**, *62*, 102643. https://doi.org/10.1016/j.algal.2022.102643.
9. Fakayode, O.A.; Aboagarib, E.A.A.; Zhou, C.; Ma, H. Co-Pyrolysis of Lignocellulosic and Macroalgae Biomasses for the Production of Biochar—A Review. *Bioresour. Technol.* **2020**, *297*, 122408. https://doi.org/10.1016/j.biortech.2019.122408.
10. Bird, M.I.; Wurster, C.M.; de Paula Silva, P.H.; Paul, N.A.; de Nys, R. Algal Biochar: Effects and Applications. *GCB Bioenergy* **2012**, *4*, 61–69. https://doi.org/10.1111/j.1757-1707.2011.01109.x.

11. Macreadie, P.I.; Trevathan-Tackett, S.M.; Baldock, J.A.; Kelleway, J.J. Converting Beach-Cast Seagrass Wrack into Biochar: A Climate-Friendly Solution to a Coastal Problem. *Sci. Total Environ.* **2017**, *574*, 90–94. https://doi.org/10.1016/j.scitotenv.2016.09.021.
12. Méndez, A.; Gascó, G.; Ruiz, B.; Fuente, E. Hydrochars from Industrial Macroalgae "Gelidium Sesquipedale" Biomass Wastes. *Bioresour. Technol.* **2019**, *275*, 386–393. https://doi.org/10.1016/j.biortech.2018.12.074.
13. Sun, J.; Norouzi, O.; Mašek, O. A State-of-the-Art Review on Algae Pyrolysis for Bioenergy and Biochar Production. *Bioresour. Technol.* **2022**, *346*, 126258. https://doi.org/10.1016/j.biortech.2021.126258.
14. Antunes, E.; Vuppaladadiyam, A.K.; Kumar, R.; Vuppaladadiyam, V.S.S.; Sarmah, A.; Anwarul Islam, M.; Dada, T. A Circular Economy Approach for Phosphorus Removal Using Algae Biochar. *Clean. Circ. Bioeconomy* **2022**, *1*, 100005. https://doi.org/10.1016/j.clcb.2022.100005.
15. Jung, K.W.; Jeong, T.U.; Kang, H.J.; Ahn, K.H. Characteristics of Biochar Derived from Marine Macroalgae and Fabrication of Granular Biochar by Entrapment in Calcium-Alginate Beads for Phosphate Removal from Aqueous Solution. *Bioresour. Technol.* **2016**, *211*, 108–116. https://doi.org/10.1016/j.biortech.2016.03.066.
16. Michalak, I.; Baśladyńska, S.; Mokrzycki, J.; Rutkowski, P. Biochar from a Freshwater Macroalga as a Potential Biosorbent for Wastewater Treatment. *Water* **2019**, *11*, 4–6. https://doi.org/10.3390/w11071390.
17. Katakula, A.A.N.; Gawanab, W.; Itanna, F.; Mupambwa, H.A. The Potential Fertilizer Value of Namibian Beach-Cast Seaweed (*Laminaria pallida* and *Gracilariopsis funicularis*) Biochar as a Nutrient Source in Organic Agriculture. *Sci. Afr.* **2020**, *10*, e00592. https://doi.org/10.1016/j.sciaf.2020.e00592.
18. Roberts, D.A.; Paul, N.A.; Dworjanyn, S.A.; Bird, M.I.; De Nys, R. Biochar from Commercially Cultivated Seaweed for Soil Amelioration. *Sci. Rep.* **2015**, *5*, 1–6. https://doi.org/10.1038/srep09665.
19. Lee, X.J.; Ong, H.C.; Gan, Y.Y.; Chen, W.H.; Mahlia, T.M.I. State of Art Review on Conventional and Advanced Pyrolysis of Macroalgae and Microalgae for Biochar, Bio-Oil and Bio-Syngas Production. *Energy Convers. Manag.* **2020**, *210*, 112707. https://doi.org/10.1016/j.enconman.2020.112707.
20. Dang, B.T.; Ramaraj, R.; Huynh, K.P.H.; Le, M.V.; Tomoaki, I.; Pham, T.T.; Hoang Luan, V.; Thi Le Na, P.; Tran, D.P.H. Current Application of Seaweed Waste for Composting and Biochar: A Review. *Bioresour. Technol.* **2023**, *375*, 128830. https://doi.org/10.1016/j.biortech.2023.128830.
21. Pimentel-Almeida, W.; Itokazu, A.G.; Bazani, H.A.G.; Maraschin, M.; Rodrigues, O.H.C.; Corrêa, R.G.; Lopes, S.; Almerindo, G.I.; Moresco, R. Beach-Cast Sargassum Cymosum Macroalgae: Biochar Production and Apply to Adsorption of Acetaminophen in Batch and Fixed-Bed Adsorption Processes. *Environ. Technol.* **2023**, *44*, 974–987. https://doi.org/10.1080/09593330.2021.1989058.
22. Campos, P.; Miller, A.Z.; Knicker, H.; Costa-Pereira, M.F.; Merino, A.; De la Rosa, J.M. Chemical, Physical and Morphological Properties of Biochars Produced from Agricultural Residues: Implications for Their Use as Soil Amendment. *Waste Manag.* **2020**, *105*, 256–267. https://doi.org/10.1016/j.wasman.2020.02.013.
23. Lehmann, J.; Joseph, S. Biochar for Environmental Management : An Introduction. In *Biochar for Environmental Management*; Routledge: London, UK; 2015; Volume 1, pp. 1–13, ISBN 9781844076581.
24. Oliveira, F.R.; Patel, A.K.; Jaisi, D.P.; Adhikari, S.; Lu, H.; Khanal, S.K. Environmental Application of Biochar: Current Status and Perspectives. *Bioresour. Technol.* **2017**, *246*, 110–122.
25. Igalavithana, A.D.; Mandal, S.; Niazi, N.K.; Vithanage, M.; Parikh, S.J.; Mukome, F.N.D.; Rizwan, M.; Oleszczuk, P.; Al-Wabel, M.; Bolan, N.; et al. Advances and Future Directions of Biochar Characterization Methods and Applications. *Crit. Rev. Environ. Sci. Technol.* **2017**, *47*, 2275–2330. https://doi.org/10.1080/10643389.2017.1421844.
26. García Tasende, M.; Peteiro, C. Explotación de Las Macroalgas Marinas: Galicia Como Caso de Estudio Hacia Una Gestión Sostenible de Los Recursos. *Ambienta* **2015**, *111*, 116–132.
27. Ciesielski, H.; Sterckeman, T. Determination of Cation Exchange Capacity and Exchangeable Cations in Soils by Means of Cobalt Hexamine Trichloride. Effets of Experimental Conditions. *Agron. Agric. Environ.* **1997**, *17*, 1–7.
28. Nelson, D.W.; Sommers, L.E. Total Carbon, Organic Carbon , and Organic Matter. In *Methods of Soil Analysis Part 3—Chemical Methods*; Soil Science Society of America and American Society of Agronomy: Madison, WI, USA, 1996; pp. 961–1009.
29. Cárdenas-Aguiar, E.; Méndez, A.; Paz-Ferreiro, J.; Gascó, G. The Effects of Rabbit Manure-Derived Biochar on Soil Health and Quality Attributes of Two Mine Tailings. *Sustainability* **2022**, *14*, 1866. https://doi.org/10.3390/su14031866.
30. Channiwala, S.A.; Parikh, P.P. A Unified Correlation for Estimating HHV of Solid, Liquid and Gaseous Fuels. *Fuel* **2002**, *81*, 1051–1063. https://doi.org/10.1016/S0016-2361(01)00131-4.
31. Element, C.A.S. Method 3051A Microwave Assisted Acid Digestion of Sediments, Sludges, Soils and Oils. *Z. Für Anal. Chem.* **2007**, *111*, 362–366.
32. Wong, J.W.C.; Ogbonnaya, U.O. Biochar Porosity: A Nature-Based Dependent Parameter to Deliver Microorganisms to Soils for Land Restoration. *Environ. Sci. Pollut. Res.* **2021**, *28*, 46894–46909. https://doi.org/10.1007/s11356-021-14803-8.
33. IUPAC Reporting Physisorption Data for Gas/Solid Systems with Special Reference to the Determination of Surface Area and Porosity (Recommendations 1984). *Pure Appl. Chem.* **1985**, *57*, 603–619. https://doi.org/10.1002/pola.26338.
34. Leng, L.; Xiong, Q.; Yang, L.; Li, H.; Zhou, Y.; Zhang, W.; Jiang, S.; Li, H.; Huang, H. An Overview on Engineering the Surface Area and Porosity of Biochar. *Sci. Total Environ.* **2021**, *763*, 144204. https://doi.org/10.1016/j.scitotenv.2020.144204.

35. Cárdenas-Aguiar, E.; Ruiz, B.; Fuente, E.; Gascó, G.; Méndez, A. Improving Mining Soil Phytoremediation with Sinapis Alba by Addition of Hydrochars and Biochar from Manure Wastes. *Waste Biomass Valorization* **2020**, *11*, 5197–5210. https://doi.org/10.1007/s12649-020-00999-2.
36. Afseth, N.K.; Kohler, A. Extended Multiplicative Signal Correction in Vibrational Spectroscopy, a Tutorial. *Chemom. Intell. Lab. Syst.* **2012**, *117*, 92–99. https://doi.org/10.1016/j.chemolab.2012.03.004.
37. Liland, K.H. *EMSC: Extended Multiplicative Signal Correction*, R Package version 0.9.4; 2021.
38. Kothawala, D.N.; Murphy, K.R.; Stedmon, C.A.; Weyhenmeyer, G.A.; Tranvik, L.J. Inner Filter Correction of Dissolved Organic Matter Fluorescence. *Limnol. Oceanogr. Methods* **2013**, *11*, 616–630. https://doi.org/10.4319/lom.2013.11.616.
39. Lakowicz, J.R. *Principles of Fluorescence Spectroscopy*, 3rd ed.; Springer: Baltimore, MD, USA, 2013.
40. Borisover, M.; Laor, Y.; Parparov, A.; Bukhanovsky, N.; Lado, M. Spatial and Seasonal Patterns of Fluorescent Organic Matter in Lake Kinneret (Sea of Galilee) and Its Catchment Basin. *Water Res.* **2009**, *43*, 3104–3116. https://doi.org/10.1016/j.watres.2009.04.039.
41. Holbrook, R.D.; Derose, P.C.; Leigh, S.D.; Rukhin, A.L.; Heckert, N.A. Excitation-Emission Matrix Fluorescence Spectroscopy for Natural Organic Matter Characterization: A Quantitative Evaluation of Calibration and Spectral Correction Procedures. *Appl. Spectrosc.* **2006**, *60*, 791–799. https://doi.org/10.1366/000370206777886973.
42. WRB, I.W.G. *World Reference Base for Soil Resources. International Soil Classification System for Naming Soils and Creating Legends for Soil Maps*, 4th, ed.; International Union of Soil Sciences (IUSS): Vienna, Austria, 2022; ISBN 9798986245119.
43. Soil Survey Staff Keys to Soil Taxonomy. *Soil Conserv. Serv.* **2014**, *12*, 410.
44. Cade-Menun, B.J.; Elkin, K.R.; Liu, C.W.; Bryant, R.B.; Kleinman, P.J.A.; Moore, P.A. Characterizing the Phosphorus Forms Extracted from Soil by the Mehlich III Soil Test. *Geochem. Trans.* **2018**, *19*, 1–17. https://doi.org/10.1186/s12932-018-0052-9.
45. Brewer, C.E.; Chuang, V.J.; Masiello, C.A.; Gonnermann, H.; Gao, X.; Dugan, B.; Driver, L.E.; Panzacchi, P.; Zygourakis, K.; Davies, C.A. New Approaches to Measuring Biochar Density and Porosity. *Biomass Bioenergy* **2014**, *66*, 176–185. https://doi.org/10.1016/j.biombioe.2014.03.059.
46. Tsai, W.T.; Liu, S.C.; Hsieh, C.H. Preparation and Fuel Properties of Biochars from the Pyrolysis of Exhausted Coffee Residue. *J. Anal. Appl. Pyrolysis* **2012**, *93*, 63–67. https://doi.org/10.1016/j.jaap.2011.09.010.
47. Yuan, J.H.; Xu, R.K.; Zhang, H. The Forms of Alkalis in the Biochar Produced from Crop Residues at Different Temperatures. *Bioresour. Technol.* **2011**, *102*, 3488–3497. https://doi.org/10.1016/j.biortech.2010.11.018.
48. Shinogi, Y.; Kanri, Y. Pyrolysis of Plant, Animal and Human Waste: Physical and Chemical Characterization of the Pyrolytic Products. *Bioresour. Technol.* **2003**, *90*, 241–247. https://doi.org/10.1016/S0960-8524(03)00147-0.
49. Ronsse, F.; van Hecke, S.; Dickinson, D.; Prins, W. Production and Characterization of Slow Pyrolysis Biochar: Influence of Feedstock Type and Pyrolysis Conditions. *GCB Bioenergy* **2013**, *5*, 104–115. https://doi.org/10.1111/gcbb.12018.
50. Bartoli, M.; Troiano, M.; Giudicianni, P.; Amato, D.; Giorcelli, M.; Solimene, R.; Tagliaferro, A. Effect of Heating Rate and Feedstock Nature on Electrical Conductivity of Biochar and Biochar-Based Composites. *Appl. Energy Combust. Sci.* **2022**, *12*, 100089. https://doi.org/10.1016/j.jaecs.2022.100089.
51. Nanda, S.; Dalai, A.K.; Berruti, F.; Kozinski, J.A. Biochar as an Exceptional Bioresource for Energy, Agronomy, Carbon Sequestration, Activated Carbon and Specialty Materials. *Waste Biomass Valorization* **2016**, *7*, 201–235. https://doi.org/10.1007/s12649-015-9459-z.
52. Chen, B.; Gu, Z.; Wu, M.; Ma, Z.; Lim, H.R.; Khoo, K.S.; Show, P.L. Advancement Pathway of Biochar Resources from Macroalgae Biomass: A Review. *Biomass Bioenergy* **2022**, *167*, 106650. https://doi.org/10.1016/j.biombioe.2022.106650.
53. Lago, B.C.; Silva, C.A.; Melo, L.C.A.; de Morais, E.G. Predicting Biochar Cation Exchange Capacity Using Fourier Transform Infrared Spectroscopy Combined with Partial Least Square Regression. *Sci. Total Environ.* **2021**, *794*, 148762. https://doi.org/10.1016/j.scitotenv.2021.148762.
54. Maddi, B.; Viamajala, S.; Varanasi, S. Comparative Study of Pyrolysis of Algal Biomass from Natural Lake Blooms with Lignocellulosic Biomass. *Bioresour. Technol.* **2011**, *102*, 11018–11026. https://doi.org/10.1016/j.biortech.2011.09.055.
55. Estela, M.C.C.B.; Juliana, S.; Matos, T.T.S.; Mayara, R.F. Effect of Surface and Porosity of Biochar on Water Holding Capacity Aiming Indirectly at Preservation of the Amazon Biome. *Nat. Sci. Reports* **2018**, *8*, 10677. https://doi.org/10.1038/s41598-018-28794-z.
56. Zhang, C.; Zhang, L.; Gao, J.; Zhang, S.; Liu, Q.; Duan, P.; Hu, X. Evolution of the Functional Groups/Structures of Biochar and Heteroatoms during the Pyrolysis of Seaweed. *Algal Res.* **2020**, *48*, 101900. https://doi.org/10.1016/j.algal.2020.101900.
57. Lataf, A.; Jozefczak, M.; Vandecasteele, B.; Viaene, J.; Schreurs, S.; Carleer, R.; Yperman, J.; Marchal, W.; Cuypers, A.; Vandamme, D. The Effect of Pyrolysis Temperature and Feedstock on Biochar Agronomic Properties. *J. Anal. Appl. Pyrolysis* **2022**, *168*, 105728. https://doi.org/10.1016/j.jaap.2022.105728.
58. Waqas, M.; Aburiazaiza, A.S.; Miandad, R.; Rehan, M.; Barakat, M.A.; Nizami, A.S. Development of Biochar as Fuel and Catalyst in Energy Recovery Technologies. *J. Clean. Prod.* **2018**, *188*, 477–488. https://doi.org/10.1016/j.jclepro.2018.04.017.
59. Parsa, M.; Jalilzadeh, H.; Pazoki, M.; Ghasemzadeh, R.; Abduli, M.A. Hydrothermal Liquefaction of Gracilaria Gracilis and Cladophora Glomerata Macro-Algae for Biocrude Production. *Bioresour. Technol.* **2018**, *250*, 26–34. https://doi.org/10.1016/j.biortech.2017.10.059.
60. Liu, K. Characterization of Ash in Algae and Other Materials by Determination of Wet Acid Indigestible Ash and Microscopic Examination. *Algal Res.* **2017**, *25*, 307–321. https://doi.org/10.1016/j.algal.2017.04.014.

61. Siatecka, A.; Oleszczuk, P. Mechanism of Aging of Biochars Obtained at Different Temperatures from Sewage Sludges with Different Composition and Character. *Chemosphere* **2022**, *287*, 132258. https://doi.org/10.1016/j.chemosphere.2021.132258.
62. Takagi, H.; Maruyama, K.; Yoshizawa, N.; Yamada, Y.; Sato, Y. XRD Analysis of Carbon Stacking Structure in Coal during Heat Treatment. *Fuel* **2004**, *83*, 2427–2433. https://doi.org/10.1016/j.fuel.2004.06.019.
63. Zhu, S.; Huang, X.; Ma, F.; Wang, L.; Duan, X.; Wang, S. Catalytic Removal of Aqueous Contaminants on N-Doped Graphitic Biochars: Inherent Roles of Adsorption and Nonradical Mechanisms. *Environ. Sci. Technol.* **2018**, *52*, 8649–8658. https://doi.org/10.1021/acs.est.8b01817.
64. Traoré, M.; Kaal, J.; Martínez Cortizas, A. Application of FTIR Spectroscopy to the Characterization of Archeological Wood. *Spectrochim. Acta—Part A Mol. Biomol. Spectrosc.* **2016**, *153*, 63–70. https://doi.org/10.1016/j.saa.2015.07.108.
65. Matamala, R.; Calderón, F.J.; Jastrow, J.D.; Fan, Z.; Hofmann, S.M.; Michaelson, G.J.; Mishra, U.; Ping, C.L. Influence of Site and Soil Properties on the DRIFT Spectra of Northern Cold-Region Soils. *Geoderma* **2017**, *305*, 80–91. https://doi.org/10.1016/j.geoderma.2017.05.014.
66. Abdulla, H.A.N.; Minor, E.C.; Dias, R.F.; Hatcher, P.G. Changes in the Compound Classes of Dissolved Organic Matter along an Estuarine Transect: A Study Using FTIR and 13C NMR. *Geochim. Cosmochim. Acta* **2010**, *74*, 3815–3838. https://doi.org/10.1016/j.gca.2010.04.006.
67. Margenot, A.J.; Calderón, F.J.; Bowles, T.M.; Parikh, S.J.; Jackson, L.E. Soil Organic Matter Functional Group Composition in Relation to Organic Carbon, Nitrogen, and Phosphorus Fractions in Organically Managed Tomato Fields. *Soil Sci. Soc. Am. J.* **2015**, *79*, 772–782. https://doi.org/10.2136/sssaj2015.02.0070.
68. Guo, M.; Chorover, J. Transport and Fractionation of Dissolved Organic Matter in Soil Columns. *Soil Sci.* **2003**, *168*, 108–118. https://doi.org/10.1097/00010694-200302000-00005.
69. Oren, A.; Chefetz, B. Sorptive and Desorptive Fractionation of Dissolved Organic Matter by Mineral Soil Matrices. *J. Environ. Qual.* **2012**, *41*, 526–533. https://doi.org/10.2134/jeq2011.0362.
70. Parikh, S.J.; Goyne, K.W.; Margenot, A.J.; Mukome, F.N.D.; Calderón, F.J. Chapter One-Soil Chemical Insights Provided through Vibrational Spectroscopy. In *Advances in Agronomy*; Donald, L.S., Ed.; Academic Press: Cambridge, MA, USA, 2014; Volume 126, pp. 1–148, ISBN 9780128001325.
71. Tinti, A.; Tugnoli, V.; Bonora, S.; Francioso, O. Recent Applications of Vibrational Mid-Infrared (IR) Spectroscopy for Studying Soil Components: A Review. *J. Cent. Eur. Agric.* **2015**, *16*, 1–22. https://doi.org/10.5513/JCEA01/16.1.1535.
72. Mukherjee, A.; Zimmerman, A.R. Organic Carbon and Nutrient Release from a Range of Laboratory-Produced Biochars and Biochar-Soil Mixtures. *Geoderma* **2013**, *193–194*, 122–130. https://doi.org/10.1016/j.geoderma.2012.10.002.
73. Cao, Q.; An, T.; Xie, J.; Liu, Y.; Xing, L.; Ling, X.; Chen, C. Insight to the Physiochemical Properties and DOM of Biochar under Different Pyrolysis Temperature and Modification Conditions. *J. Anal. Appl. Pyrolysis* **2022**, *166*, 105590. https://doi.org/10.1016/j.jaap.2022.105590.
74. Weishaar, J.L.; Aiken, G.R.; Bergamaschi, B.A.; Fram, M.S.; Fujii, R.; Mopper, K. Evaluation of Specific Ultraviolet Absorbance as an Indicator of the Chemical Composition and Reactivity of Dissolved Organic Carbon. *Environ. Sci. Technol.* **2003**, *37*, 4702–4708. https://doi.org/10.1021/es030360x.
75. Trompowsky, P.M.; De Melo Benites, V.; Madari, B.E.; Pimenta, A.S.; Hockaday, W.C.; Hatcher, P.G. Characterization of Humic like Substances Obtained by Chemical Oxidation of Eucalyptus Charcoal. *Org. Geochem.* **2005**, *36*, 1480–1489. https://doi.org/10.1016/j.orggeochem.2005.08.001.
76. Knicker, H. How Does Fire Affect the Nature and Stability of Soil Organic Nitrogen and Carbon? A Review. *Biogeochemistry* **2007**, *85*, 91–118. https://doi.org/10.1007/s10533-007-9104-4.
77. Chen, W.; Westerhoff, P.; Leenheer, J.A.; Booksh, K. Fluorescence Excitation-Emission Matrix Regional Integration to Quantify Spectra for Dissolved Organic Matter. *Environ. Sci. Technol.* **2003**, *37*, 5701–5710. https://doi.org/10.1021/es034354c.
78. Balmuk, G.; Videgain, M.; Manyà, J.J.; Duman, G.; Yanik, J. Effects of Pyrolysis Temperature and Pressure on Agronomic Properties of Biochar. *J. Anal. Appl. Pyrolysis* **2023**, *169*, 105858. https://doi.org/10.1016/j.jaap.2023.105858.
79. Hass, A.; Gonzalez, J.M.; Lima, I.M.; Godwin, H.W.; Halvorson, J.J.; Boyer, D.G. Chicken Manure Biochar as Liming and Nutrient Source for Acid Appalachian Soil. *J. Environ. Qual.* **2012**, *41*, 1096–1106. https://doi.org/10.2134/jeq2011.0124.
80. Sun, Z.; Hu, Y.; Shi, L.; Li, G.; Pang, Z.; Liu, S.; Chen, Y.; Jia, B. Effects of Biochar on Soil Chemical Properties: A Global Meta-Analysis of Agricultural Soil. *Plant Soil Environ.* **2022**, *68*, 272–289. https://doi.org/10.17221/522/2021-PSE.